

# Search for Dijet Resonances in 7 TeV $pp$ Collisions at CMS

The CMS Collaboration  
CERN

(Dated: September 24, 2010)

We have used data corresponding to an integrated luminosity of  $2.9 \text{ pb}^{-1}$  collected with the CMS experiment at the Large Hadron Collider to search for narrow resonances in the dijet mass spectrum. Upper limits are presented on the product of the resonance cross section, branching fraction into dijets, and acceptance. These generic limits are used to exclude new particles predicted in the following specific models at the 95% confidence level: string resonances with mass less than 2.50 TeV, excited quarks with mass less than 1.58 TeV, and axigluons, colorons, and  $E_6$  diquarks in specific mass intervals, extending previously published limits on all these models.

Two energetic jets (dijets) arise in proton-proton collisions when outgoing scattered partons manifest themselves as hadronic jets. The dijet mass spectrum predicted by Quantum Chromodynamics (QCD) falls smoothly and steeply with increasing dijet mass. Many extensions of the Standard Model predict the existence of new massive objects that couple to quarks ( $q$ ) and gluons ( $g$ ), and result in resonant structures in the dijet mass spectrum. In this Letter we report a search for narrow resonances in the dijet mass spectrum, measured with the Compact Muon Solenoid (CMS) detector [1] at the CERN Large Hadron Collider, at a proton-proton collision energy of  $\sqrt{s} = 7 \text{ TeV}$ .

In addition to this generic search, we search for manifestations of eight specific models of narrow s-channel dijet resonances. First, string resonances ( $S$ ) are Regge excitations of the quarks and gluons in string theory, with multiple mass-degenerate spin states and quantum numbers [2, 3]. String resonances with mass  $\sim 2 \text{ TeV}$  are expected to decay predominantly to  $qg$  (91%) with small amounts of  $gg$  (5.5%) and  $q\bar{q}$  (3.5%). Second, if quarks are composite particles then excited states are expected, and we search for mass-degenerate excited quarks ( $q^*$ ) that decay to  $qg$  [4]. The compositeness scale is set to be equal to the mass of the excited quark. Third, in a model where the symmetry group  $SU(3)$  of QCD is replaced by the chiral symmetry  $SU(3)_L \times SU(3)_R$ , there are axial vector particles called axigluons ( $A$ ) which decay to  $q\bar{q}$  [5]. Fourth, the flavor-universal coloron model also embeds the  $SU(3)$  of QCD in a larger gauge group, and predicts the presence of a color-octet coloron ( $C$ ) which decays to  $q\bar{q}$  [6]. Fifth, a grand unified theory based on the  $E_6$  gauge group predicts the presence of scalar diquarks ( $D$ ) which decay to  $qg$  and  $q\bar{q}$  [7]. Sixth, the Randall-Sundrum (RS) model of extra dimensions predicts massive gravitons ( $G$ ) which decay to  $q\bar{q}$  and  $gg$  [8]. For the RS graviton, the value of the dimensionless coupling  $\kappa/\overline{M}_{\text{Pl}}$  is set herein to 0.1. Seventh and eighth, models that propose new gauge symmetries often predict new gauge bosons ( $W'$  and  $Z'$ ) which decay to  $q\bar{q}$  [9]. The  $W'$  and  $Z'$  resonances are assumed to have standard-model-like couplings and to have fractional widths equal to the corresponding standard model  $W$  and  $Z$  bosons.

A detailed description of the CMS experiment can be found elsewhere [1]. The CMS coordinate system has the origin at the center of the detector; the  $z$ -axis points along the direction of the counterclockwise beam, with the transverse plane perpendicular to the beam. We define  $\phi$  to be the azimuthal angle,  $\theta$  to be the polar angle and the pseudorapidity as  $\eta \equiv -\ln(\tan[\theta/2])$ . The central feature of the CMS apparatus is a superconducting solenoid, of 6 m internal diameter. Within the field volume are the silicon pixel and strip tracker ( $|\eta| < 2.4$ ), and the barrel and endcap calorimeters ( $|\eta| < 3$ ): a lead tungstate crystal electromagnetic calorimeter (ECAL) and a brass-scintillator hadronic calorimeter (HCAL). Outside the field volume, in the forward region, there is an iron-quartz fiber calorimeter ( $3 < |\eta| < 5$ ). The ECAL and HCAL cells are grouped into towers, projecting radially outward from the origin, for triggering purposes and to facilitate the jet reconstruction. In the region  $|\eta| < 1.74$  these projective calorimeter towers have segmentation  $\Delta\eta = \Delta\phi = 0.087$ , and the  $\eta$  and  $\phi$  width progressively increases at higher values of  $\eta$ . The energy depositions measured in the HCAL and ECAL within each projective tower are summed to find the calorimeter tower energy. Towers with  $|\eta| < 1.3$  contain only cells from the barrel calorimeters, towers in the transition region  $1.3 < |\eta| < 1.5$  contain a mixture of barrel and endcap cells, and towers in the region  $1.5 < |\eta| < 3.0$  contain only cells from the endcap calorimeters.

The integrated luminosity of the selected data sample used for this analysis is  $2.9 \pm 0.3 \text{ pb}^{-1}$  [11]. A single-jet trigger is used in both the online hardware-level (L1) and software-level (HLT) trigger system [1] to select an unprescaled sample of events with a nominal jet transverse energy threshold at HLT of 50 GeV. The trigger efficiency versus dijet mass for this analysis is measured from the data and is greater than 99.5% for dijet masses above 220 GeV [12].

Jets are reconstructed using the anti- $k_T$  algorithm [13] with a distance parameter  $R = 0.7$ . The reconstructed jet energy,  $E$ , is defined as the scalar sum of the calorimeter tower energies inside the jet. The jet momentum,  $\vec{p}$ , is the corresponding vector sum of the tower energies using the tower directions. The  $E$  and  $\vec{p}$  of a reconstructed

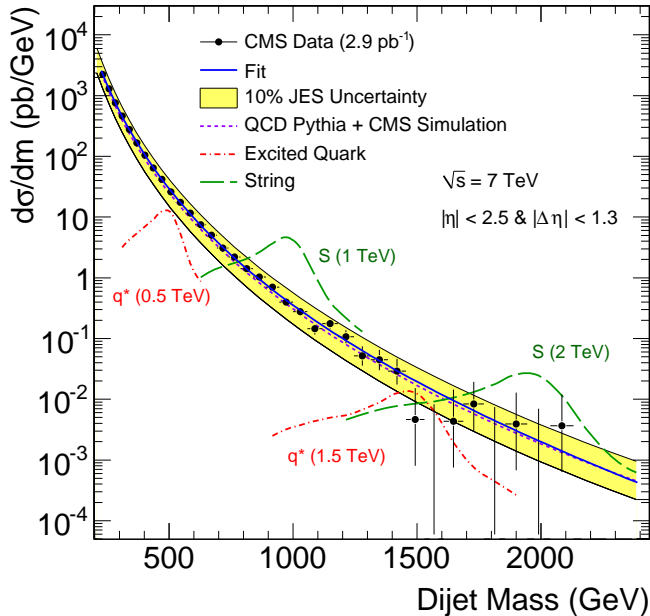


FIG. 1. Measured cross section (points) as a function of the dijet mass compared to a smooth fit (solid blue) and to simulations [10] of QCD (short-dashed purple), excited quark signals (dot-dashed red), and string resonance signals (long-dashed green) in the CMS detector. The yellow band shows the sensitivity to a 10% systematic uncertainty on the jet energy scale (JES).

jet are corrected as a function of transverse momentum ( $p_T$ ) and  $\eta$  for the non-linearity and inhomogeneity of the calorimeter response. The correction is between 43% and 15% for jets with corrected  $p_T$  between 0.1 and 1.0 TeV in the region  $|\eta| < 1.3$ . The jet energy corrections were determined and validated using Monte Carlo, test beam data, and collision data [14].

The dijet system is composed of the two jets with the highest  $p_T$  in an event (leading jets). We require that the pseudorapidity separation of the two leading jets,  $\Delta\eta = \eta_1 - \eta_2$ , satisfies  $|\Delta\eta| < 1.3$ , and also require that both jets be in the region  $|\eta| < 2.5$ . These  $\eta$  cuts maximize the search sensitivity for isotropic decays of dijet resonances in the presence of QCD background. The dijet mass is given by  $m = \sqrt{(E_1 + E_2)^2 - (\vec{p}_1 + \vec{p}_2)^2}$ . We select events with  $m > 220$  GeV without any requirements on jet  $p_T$ .

To remove possible instrumental and non-collision backgrounds in the selected sample, the following selections are made. Events in the sample are required to have a reconstructed primary vertex with  $|z| < 24$  cm. Jets are required to have a minimum of 1% of their total energy detected in the ECAL, a minimum multiplicity of two calorimeter cells, ECAL or HCAL, and a maximum of 98% of the total energy occurring in a single photode-

tection device of the hadron calorimeter readout. The jet identification criteria remove 0.1% of the events passing the pseudorapidity constraints and the dijet mass threshold.

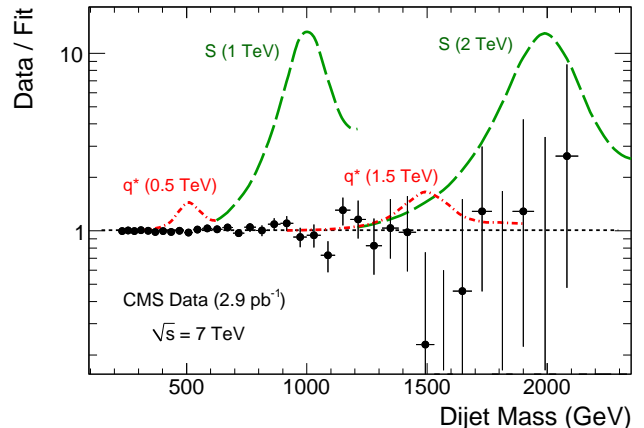


FIG. 2. The ratio (points) between the dijet mass data and the smooth background fit is compared to the respective simulated ratio for excited quark signals (dot-dashed red) and string resonance signals (long-dashed green) in the CMS detector.

In Fig. 1 we present the inclusive dijet mass distribution for  $pp \rightarrow 2$  leading jets +  $X$ , where  $X$  can be anything, including additional jets. We plot the measured differential cross section versus dijet mass in bins approximately equal to the dijet mass resolution. The data are compared to a QCD prediction from PYTHIA [10], which includes a simulation of the CMS detector and the jet energy corrections. The prediction uses CTEQ6L1 parton distribution functions [15] and a renormalization scale  $\mu = p_T$ . The data agree with the PYTHIA prediction within the systematic uncertainties of the measurement. To test the smoothness of our measured cross section as a function of dijet mass, we fit the data with the parameterization:

$$\frac{d\sigma}{dm} = \frac{P_0(1 - m/\sqrt{s})^{P_1}}{(m/\sqrt{s})^{P_2 + P_3 \ln(m/\sqrt{s})}}, \quad (1)$$

with four free parameters  $P_0$ ,  $P_1$ ,  $P_2$  and  $P_3$ . This parameterization has been used by two prior searches to fit both data and QCD predictions [16, 17]. In Fig. 1 we show both the data and the fit, which has a  $\chi^2$  of 32 for 31 degrees of freedom. In Fig. 2 we show the ratio between the data and the fit. The data are well described by the smooth parameterization.

We search for narrow resonances, for which the natural resonance width is negligible compared to the CMS dijet mass resolution. In Figs. 1 and 2 we show the predicted dijet mass distribution for string resonances and

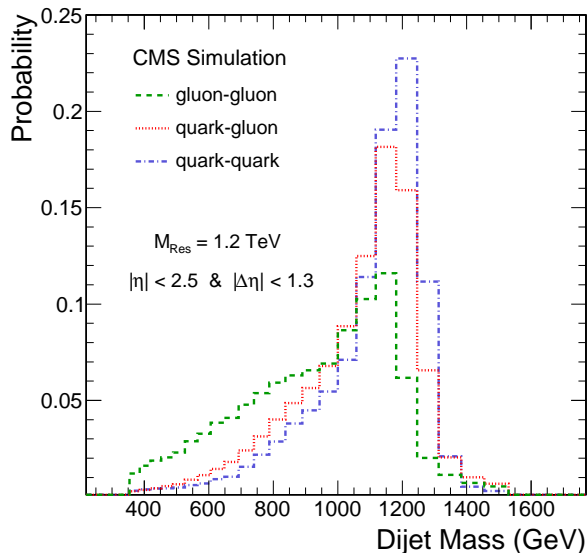


FIG. 3. Simulation of the expected dijet mass distributions in the CMS detector from a narrow 1.2 TeV resonance of type quark-quark (dot-dashed blue), quark-gluon (dotted red), and gluon-gluon (dashed green).

excited quarks using the PYTHIA Monte Carlo [10] and the CMS detector simulation. The mass resolution exhibits a Gaussian core from jet energy resolution and a long tail towards low mass from QCD radiation. The dijet mass distribution of narrow dijet resonances depends on the type of partons coming from the resonance decay, because this affects both the amount of radiation and the final state jet response in the CMS detector. This can be seen in Fig. 3, where we show examples of the predicted dijet mass distribution of resonances from three different parton pairings:  $qq$  (or  $q\bar{q}$ ) resonances from the process  $G \rightarrow q\bar{q}$  [8],  $qg$  resonances from the process  $q^* \rightarrow qg$  [4], and  $gg$  resonances from the process  $G \rightarrow gg$  [8]. The dijet mass resolution varies from 10% at 0.5 TeV to 6% at 2.5 TeV for  $qg$  resonances. These resonance shapes are approximately valid for any resonance model involving these pairs of partons, assuming that the resonance's natural half-width ( $\Gamma/2$ ) is small compared to the dijet mass resolution. The width of dijet resonances increases with the number of gluons in the final state, primarily because gluons emit more radiation than quarks. The peak value of the dijet mass for the resonance decreases with the number of final state gluons, primarily due to the lower response of the CMS detector to gluon jets than to quark jets [18]. The generic jet corrections, which we apply to both the data and all simulations, are for the mixture of quarks and gluons expected in QCD dijet production. There is no indication of narrow resonances in our data in Figs. 1 and 2.

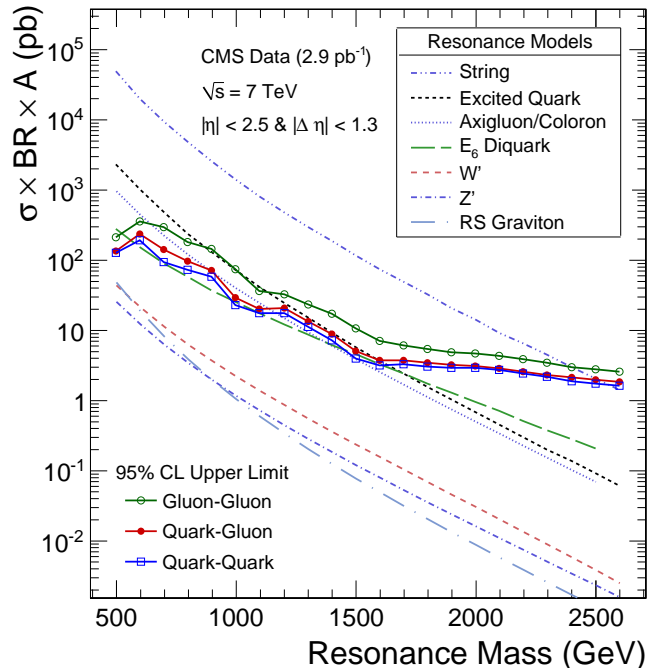


FIG. 4. 95% CL upper limits on  $\sigma \times \text{BR} \times A$  for dijet resonances of type gluon-gluon (open circles), quark-gluon (solid circles), and quark-quark (open boxes) compared to theoretical predictions for string resonances [2], excited quarks [4], axigluons [5], colorons [6],  $E_6$  diquarks [7], new gauge bosons  $W'$  and  $Z'$  [9], and Randall-Sundrum gravitons [8].

We use the dijet mass data points, the background parameterization, and the dijet resonance shapes to set specific limits on new particles decaying to the parton pairs  $qq$  (or  $q\bar{q}$ ),  $qg$ , and  $gg$ . For setting upper limits on the resonance production cross section, before accounting for systematic uncertainties, we begin with a Bayesian formalism with a uniform prior for the signal cross section. We calculate the posterior probability density as a function of resonance cross section independently at 22 different values of the resonance mass from 0.5 to 2.6 TeV in 0.1 TeV steps from which we find initial 95% confidence level (CL) upper limits on the cross section, including only statistical uncertainties. The dominant sources of systematic uncertainty are the jet energy scale (10%), the background parameterization choice, the jet energy resolution (10%), and the luminosity (11%). The jet energy scale and resolution uncertainties are conservative estimates within that measured in situ using collision data [14]. To incorporate systematic uncertainties, we use an approximate technique, which in our application is generally more conservative than a fully Bayesian treatment. The posterior probability density for the cross section is broadened from that without systematic uncer-

tainties by convoluting with a Gaussian systematic uncertainty for each resonance mass [19]. As a result, the cross section limits including systematic uncertainties increase by 17%–49% as a function of the resonance mass and type over the corresponding limits derived with statistical uncertainties alone. Table I lists the generic upper limits at the 95% CL on  $\sigma \times \text{BR} \times A$ , the product of cross section ( $\sigma$ ), branching fraction (BR), and acceptance (A), for  $qq$ ,  $qg$ , and  $gg$  resonances.

In Fig. 4 we compare these upper limits to the model predictions as a function of resonance mass. The predictions are lowest order calculations of  $\sigma \times \text{BR} \times A$  for dijets satisfying  $|\Delta\eta| < 1.3$  and  $|\eta| < 2.5$  with the CTEQ6L1 parton distributions [15]. We exclude at the 95% CL new particles in mass regions for which the theory curve lies above our upper limit for the appropriate pair of partons. For string resonances we use our limits on  $qg$  resonances to exclude at the 95% CL the mass range  $0.50 < M(S) < 2.50$  TeV. For comparison, previous cross section upper limits on dijet resonances [16] imply a limit on string resonances of about 1.4 TeV. For excited quarks we use our limits on  $qg$  resonances to exclude the mass range  $0.50 < M(q^*) < 1.58$  TeV, extending the previous exclusion of  $0.40 < M(q^*) < 1.26$  TeV [17]. For axiglucos or colorons we use our limits on  $qg$  resonances to exclude the mass intervals  $0.50 < M(A) < 1.17$  TeV and  $1.47 < M(A) < 1.52$  TeV extending the previous exclusion of  $0.12 < M(A) < 1.25$  TeV [16]. For  $E_6$  diquarks we use our limits on  $qg$  resonances to exclude the mass intervals  $0.50 < M(D) < 0.58$  TeV, and  $0.97 < M(D) < 1.08$  TeV, and  $1.45 < M(D) < 1.60$  TeV, extending the previous exclusion of  $0.29 < M(D) < 0.63$  TeV [16]. For  $W'$ ,  $Z'$  and RS gravitons we do not exclude any mass intervals. The systematic uncertainties included in this analysis reduce the excluded upper masses by roughly 0.1 TeV for each type of new particle.

In conclusion, the measured dijet mass spectrum is a smoothly falling distribution as expected within the Standard Model. We see no evidence for new particle production, present generic upper limits on the cross section times branching fraction times acceptance that can be applied to any model of dijet resonances, and set specific mass limits on string resonances, excited quarks, axiglucos, flavor universal colorons, and  $E_6$  diquarks, all of which extend previous exclusions.

We wish to congratulate our colleagues in the CERN accelerator departments for the excellent performance of the LHC machine. We thank the technical and administrative staff at CERN and other CMS institutes, and acknowledge support from: FMSR (Austria); FNRS and FWO (Belgium); CNPq, CAPES, FAPERJ, and FAPESP (Brazil); MES (Bulgaria); CERN; CAS, MoST, and NSFC (China); COLCIENCIAS (Colombia); MSES (Croatia); RPF (Cyprus); Academy of Sciences and NICPB (Estonia); Academy of Finland, ME,

TABLE I. Upper limits at the 95% CL on  $\sigma \times \text{BR} \times A$ , as a function of the new particle mass, for narrow resonances decaying to dijets with partons of type quark-quark ( $qq$ ), quark-gluon ( $qg$ ), and gluon-gluon ( $gg$ ). The limits apply to the kinematic range where both jets have pseudorapidity  $|\eta| < 2.5$  and  $|\Delta\eta| < 1.3$ .

Mass (TeV)	Upper Limit (pb)			Mass (TeV)	Upper Limit (pb)		
	qq	qg	gg		qq	qg	gg
0.5	118	134	206	1.6	3.05	3.72	6.71
0.6	182	229	339	1.7	3.13	3.64	5.88
0.7	90.7	134	281	1.8	2.92	3.41	5.37
0.8	70.8	93.5	177	1.9	2.73	3.15	4.78
0.9	52.7	71.6	142	2.0	2.71	3.02	4.39
1.0	20.3	29.0	71.4	2.1	2.50	2.84	4.15
1.1	17.0	20.1	35.1	2.2	2.20	2.55	3.69
1.2	17.0	20.4	32.5	2.3	1.96	2.28	3.32
1.3	10.5	12.9	22.8	2.4	1.79	2.08	2.94
1.4	6.77	8.71	16.4	2.5	1.67	1.93	2.74
1.5	3.71	5.02	10.3	2.6	1.55	1.80	2.50

and HIP (Finland); CEA and CNRS/IN2P3 (France); BMBF, DFG, and HGF (Germany); GSRT (Greece); OTKA and NKTH (Hungary); DAE and DST (India); IPM (Iran); SFI (Ireland); INFN (Italy); NRF and WCU (Korea); LAS (Lithuania); CINVESTAV, CONACYT, SEP, and UASLP-FAI (Mexico); PAEC (Pakistan); SCSR (Poland); FCT (Portugal); JINR (Armenia, Belarus, Georgia, Ukraine, Uzbekistan); MST and MAE (Russia); MSTD (Serbia); MICINN and CPAN (Spain); Swiss Funding Agencies (Switzerland); NSC (Taipei); TUBITAK and TAEK (Turkey); STFC (United Kingdom); DOE and NSF (USA).

- 
- [1] JINST, **0803**, S08004 (2008).
  - [2] L. A. Anchordoqui *et al.*, Phys. Rev. Lett., **101**, 241803 (2008).
  - [3] S. Cullen, M. Perelstein, and M. E. Peskin, Phys. Rev., **D62**, 055012 (2000).
  - [4] U. Baur, I. Hinchliffe, and D. Zeppenfeld, Int. J. Mod. Phys., **A2**, 1285 (1987).
  - [5] P. H. Frampton and S. L. Glashow, Phys. Lett., **B190**, 157 (1987).
  - [6] E. H. Simmons, Phys. Rev., **D55**, 1678 (1997).
  - [7] J. L. Hewett and T. G. Rizzo, Phys. Rept., **183**, 193 (1989).
  - [8] L. Randall and R. Sundrum, Phys. Rev. Lett., **83**, 4690 (1999).
  - [9] E. Eichten *et al.*, Rev. Mod. Phys., **56**, 579 (1984).
  - [10] T. Sjostrand *et al.*, Computer Physics Commun., **135**, 238 (2001).

- [11] CMS PAS EWK-10-004 (2010).
- [12] CMS PAS EXO-10-010 (2010).
- [13] M. Cacciari, G. P. Salam, and G. Soyez, *JHEP*, **04**, 063 (2008).
- [14] CMS PAS JME-10-003 (2010).
- [15] J. Pumplin *et al.*, *JHEP*, **07**, 012 (2002).
- [16] T. Aaltonen *et al.* (CDF), *Phys. Rev.*, **D79**, 112002 (2009).
- [17] G. Aad *et al.* (ATLAS), Submitted to *Phys. Rev. Lett.*, arXiv:1008.2461 [hep-ex].
- [18] CMS PAS JME-07-002 (2008).
- [19] F. Abe *et al.* (CDF), *Phys. Rev.*, **D55**, 5263 (1997).